Applied Physics Letters

RESEARCH ARTICLE | MAY 20 2026

Interplay of ferromagnetic and antiferromagnetic interactions in epitaxial Co_3ZnN

Sita Dugu ; Sharad Mahatara ; Corlyn E. Regier ; James R. Neilson ; Stephan Lany ; Rebecca W. Smaha ; Sage R. Bauers

Appl. Phys. Lett. 128, 202405 (2026)
https://doi.org/10.1063/5.0325854

AIP Publishing

Applied Physics Letters ARTICLE pubs.aip.org/aip/apl

Interplay of ferromagnetic and antiferromagnetic interactions in epitaxial Co_3ZnN

Cite as: Appl. Phys. Lett. **128**, 202405 (2026); doi: 10.1063/5.0325854
Submitted: 2 February 2026 · Accepted: 4 May 2026 ·
Published Online: 20 May 2026

Sita Dugu,[1] Sharad Mahatara,[1] Corlyn E. Regier,[2] James R. Neilson,[2,3] Stephan Lany,[1] Rebecca W. Smaha,[1,a)] and Sage R. Bauers[1,a)]

AFFILIATIONS

[1]Materials Sciences Center, National Laboratory of the Rockies, Golden, Colorado 80401, USA
[2]Department of Chemistry, Colorado State University, Fort Collins, Colorado 80523-1872, USA
[3]School of Materials Science Engineering, Colorado State University, Fort Collins, Colorado 80523-1617, USA

[a)]**Authors to whom correspondence should be addressed:** Rebecca.Smaha@nlr.gov and Sage.Bauers@nlr.gov

ABSTRACT

Antiperovskite nitrides with the general formula M_3AN have attracted significant attention due to their tunable electronic and magnetic properties. Among them are many cobalt-based compounds predicted to exhibit high thermodynamic stability and intriguing magnetic behavior. Here, we report the synthesis and magnetic characterization of epitaxial Co_3ZnN thin films grown by radio frequency sputtering on $SrTiO_3$ (STO) and MgO substrates. X-ray diffraction confirms phase-pure (00*l*)-oriented films with cube-on-cube epitaxy on STO, with a *c*-lattice parameter of 3.752 Å. Magnetic measurements reveal clear hysteresis at 2 K with a coercive field of ∼0.11 T and a small net moment of 0.108 μ_B/f.u., suggesting either a canted antiferromagnetic (AFM) or ferrimagnetic (FiM) configuration. Temperature-dependent magnetization measurements show a transition near 25 K, with strong AFM interactions with Curie–Weiss temperature $(\Theta) = -80.13$ K. Complementary density functional theory and Monte Carlo simulations indicate a ferromagnetic (FM) ground state, with the FM–AFM energy difference decreasing systematically with increasing supercell size, consistent with competition between FM and AFM/FiM interactions. These results highlight Co_3ZnN as a magnetically complex antiperovskite nitride with competing exchange interactions.

Antiperovskite (AP) nitrides with the general formula M_3AN represent a significant branch of all M_3AX AP compounds and are known for their diverse and intriguing physical properties as well as their potential multifunctionalities.[1,2] Within this family, several subclasses with 3*d* *M*-site metals have been extensively studied. For instance, Ni-based nitride Ni_3AN (A = Cu and Zn) show superconducting behavior;[3,4] Fe-based systems like Fe_3AN (A = Pd, Mn, Fe, Sn, and Ni) show nearly invariant coefficients of thermal expansion (CTEs);[5–11] Mn-based compounds, including Mn_3AN (A = Zn, Ge, Ga, and Cu), display large negative CTEs,[12,13] magnetocaloric and barocaloric effects,[14,15] spin glass (SG) behavior,[16,17] and magnetostriction;[18] and Cr-based nitrides Cr_3AN (A = Ga, Pd, Rh, and Pt) have been reported to exhibit superconductivity, SG behavior, and zero-field cooled (ZFC) exchange bias effects.[19,20]

Despite several experimental studies on M_3AN compounds, magnetic investigations of Co-based AP nitrides remain limited due to challenges in synthesizing high-quality samples such as single crystals or epitaxial films. Yet high-throughput density functional theory (DFT) calculations by Singh *et al.*[21] indicate that Co-based cubic APs are thermodynamically stable, lying on the convex hull. Recent experiments support the stability of Co-based APs and provide insight into their magnetic behavior. For example, Liu *et al.*[22] reported spin glass behavior in Co_3SnN attributed to competing antiferromagnetic (AFM) and ferromagnetic (FM) interactions arising from atomic disorder. Co_3FeN displays reversible magnetic domain structures and magnetization, and studies on bilayer thin films combining FM Co_3FeN with AFM Mn_3GaN demonstrate current-induced spin-transfer torque effects in the Mn_3GaN layer.[23]

Our prior work demonstrated the growth of another theoretically predicted Co-based AP, Co_3PdN.[24] Motivated by the successful synthesis of Co_3PdN and its high-temperature ferromagnetism (Curie temperature of $T_C \approx 560$ K), here we explore another candidate material, Co_3ZnN, identified by high-throughput DFT as lying on the convex hull of stability.[21] While phase-pure Co_3ZnN ($a = 3.764$ Å) was

recently synthesized via ammonolysis for nitrogen storage applications,[25] no studies have reported thin-film fabrication or magnetic characterization.

Here, we report the epitaxial growth of Co_3ZnN films of thickness 50 and 180 nm using RF co-sputtering and investigate their magnetic properties. We grew the Co_3ZnN films on strontium titanate (STO) and magnesium oxide (MgO) substrates by radio frequency (RF) co-sputtering in a mixture of Ar and N_2 gases. Uniform films with a final composition of $Co_{2.97}Zn_{1.01}N_{0.95}O_{0.07}$, determined for the thinner film using electron probe microanalysis (EPMA), were achieved by applying 70 W to the Co and 40 W to the Zn sources (both >99.9% pure). Thicker films were grown using identical conditions and revealed similar composition, checked via wavelength dispersive x-ray fluorescence (WD-XRF).

X-ray diffraction (XRD) patterns of the films are shown in Fig. 1(a), where only (00*l*) reflections are observed. In nitride APs, the odd (00*l*) reflections arise primarily due to the difference in scattering factors between the corner (Zn) and face-center (Co) atoms. Thus, the (001) peak [shown in the inset of Fig. 1(a)] exhibits low intensity primarily because of the similar Z values of Co and Zn. Co_3ZnN films grown on MgO (Fig. S1 in the supplementary material) also show exclusively (00*l*) reflections. This is consistent with the expected cubic $Pm\bar{3}m$ symmetry of the AP structure. We calculate the out-of-plane lattice parameter to be 3.752 Å and found no indication of tetragonal distortion. The lattice mismatch of the film is +3.56% on STO, and it increases to +10.92% on MgO, so we selected STO for further growth and characterization. Figure 1(b) shows an XRD pole figure collected from the (111) plane of Co_3ZnN. The discrete points of intensity overlap in χ/φ with the substrate's (111) poles, indicating cube-on-cube epitaxy. φ-scans collected from the film and STO substrate from [111] planes [Fig. 1(c)] also show peaks separated by 90°, consistent with the expected fourfold symmetry. This confirms a cube-on-cube relationship between the Co_3ZnN film and the (001)-oriented STO substrate [Fig. 1(d)], establishing the in-plane epitaxial relationship as $Co_3ZnN(001)[100] \parallel STO(001)[100]$.

We characterized the magnetic properties of epitaxial 180 nm thick Co_3ZnN films on STO substrates using DC magnetization and SQUID magnetometry as a function of both temperature and applied magnetic field. The sample was measured with the magnetic field aligned in-plane. Figure 2(a) shows magnetic hysteresis loops measured at various temperatures; the data are plotted after subtracting the contribution from the substrates (see Fig. S2 in the supplementary material). A clear hysteresis is observed at 2 K, and it disappears above 20 K. The film exhibits a coercive field (H_C) ~0.11 T, significantly

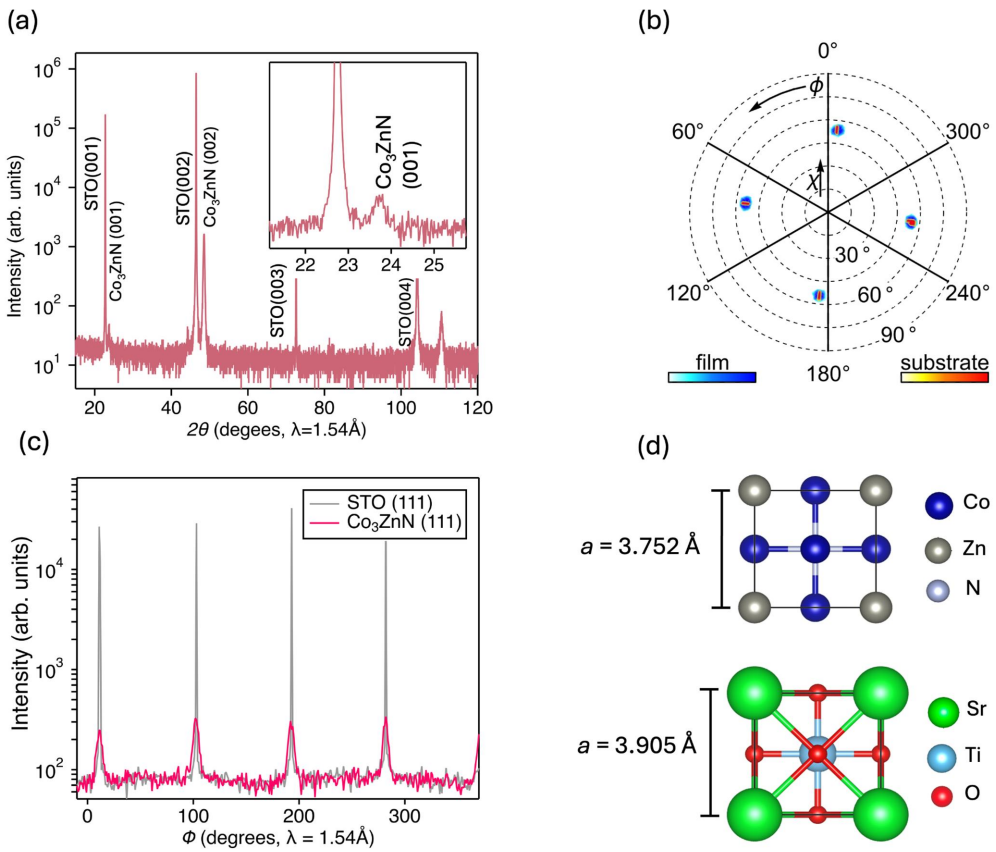

FIG. 1. (a) presents XRD data collected in ω–2θ geometry from Co_3ZnN thin films grown on the (00*l*) STO substrate [peaks at 82° and 110° are Co_3ZnN (003) and Co_3ZnN (004)]. (b) Pole figure of the Co_3ZnN (111) and STO (111) family of peaks. (c) φ-scans collected at the (111) Bragg condition for Co_3ZnN and STO. All measurements were done on 180 nm thick films. (d) Crystal structure schematics of antiperovskite Co_3ZnN and perovskite STO.

higher than that of polycrystalline Co_3PdN reported in our prior investigation.[24] However, the remanent magnetization at 2 K is approximately 20 emu/cm^3 (0.108 μ_B/f.u.), which is notably smaller than that of Co_3PdN (~550 emu/cm^3). The presence of a hysteresis loop with small net magnetization suggests that the system likely has either a canted AFM or a ferrimagnetic (FiM) ground state.

Figure 2(a) also indicates that at 300 K, slightly diamagnetic behavior is observed at lower fields ($-0.1 < \mu_0 H < 0.1$ T), above which the curve then becomes paramagnetic. This diamagnetic behavior arises from the background subtraction of STO that has a small ferromagnetic or paramagnetic response on top of a large diamagnetic background. This is known to happen with either doped STO (e.g., Pauli paramagnetism)[26] or from small concentrations of transition metal impurities. Therefore, we believe that the slight ferromagnetism observed at 300 K in Fig. 2(a) is an artifact from the STO substrate. The MH and MT raw data of the sample, including the substrate contribution, are shown in Figs. S2(a) and S2(c) in the supplementary material. Figures S2(b) and S2(d) display the MH and MT raw data of a bare STO substrate. To check this discrepancy, we have measured the magnetic properties of a film grown on a silicon substrate. The observed diamagnetic behavior is not present in the film grown on a silicon substrate [Fig. S3(a)]. Hence, the discrepancy is the result of trace impurities in the STO substrate as discussed above.

Temperature-dependent magnetization was measured under both zero-field cooled (ZFC) and field cooled (FC) conditions at applied fields of 0.05 and 0.5 T, as shown in Fig. 2(b). To estimate the transition temperature, the first derivative of the FC curve collected at 0.05 T was calculated, revealing a transition around 25 K [Fig. 2(c)]. The sharp decrease in the ZFC curve below the transition suggests AFM ordering. A pronounced bifurcation between the ZFC and FC curves is observed at low temperatures under an applied field of 0.05 T with a sharp peak in the ZFC curve at ~20 K. This bifurcation is not present in the data collected at 0.5 T. This ZFC-FC bifurcation

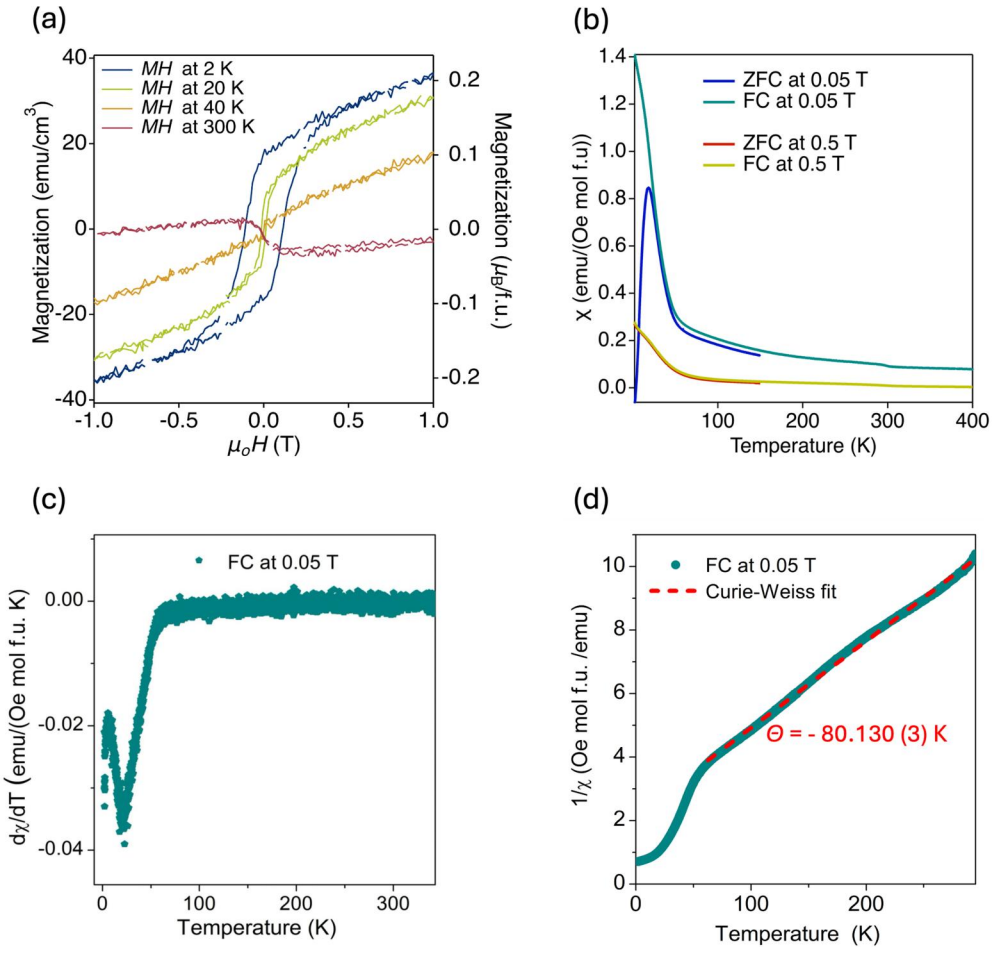

FIG. 2. (a) Magnetization vs field of Co_3ZnN film measured from 2 to 300 K. (b) Susceptibility vs temperature measured at 0.05 and 0.5 T under zero-field cooled (ZFC) and field cooled (FC) conditions. (c) First order derivative of susceptibility with respect to temperature calculated for field cooled data measured at 0.05 T. (d) Inverse susceptibility as a function of temperature with Curie–Weiss fit from 100 to 300 K for field cooled data measured at 0.05 T. The contribution of the STO has been removed (see the supplementary material for details), although the slight diamagnetism and weak ferromagnetism observed at 300 K in panel (a) is an artifact of the STO substrate.

behavior may indicate some spin glass character of the ground state, which was previously reported in Co_3SnN,[22,27] although it is also relatively common in complex antiferromagnets.

To further investigate the magnetic ordering, the FC data collected at 0.05 T were fitted to the Curie–Weiss law,[28] as shown in Fig. 2(d). A fit in the 100–300 K range yields a Weiss temperature (Θ) of −80.13(3) K, indicating strong AFM interactions in the paramagnetic regime. Overall, this is a sharp departure from the magnetic behavior observed for Co_3PdN films, which exhibit strong ferromagnetism with a T_C of 563.2(4) K.[24] However, antiferromagnetism or ferrimagnetism is quite common in the M_3AN AP family as a whole, with many Mn-based compounds displaying AFM or FiM ground states.[2]

Interestingly, Fig. 2(d) shows a pronounced kink in the inverse susceptibility (χ^{-1}) data at approximately 60 K. The steep slope of the temperature-dependent susceptibility data below this kink yet above the transition temperature (i.e., 25–50 K) suggests the emergence of short-range FM correlations near the transition temperature, consistent with the appearance of a hysteresis loop below the transition. However, the high-temperature behavior above this kink, characterized by a negative Curie–Weiss temperature (Θ), indicates that the dominant interactions in the paramagnetic regime are antiferromagnetic. Together, these results suggest competition between ferromagnetic and antiferromagnetic ordering in the system leading to a canted AFM or FiM ground state. An MT graph of the film grown on Si is shown in Fig. S3(b).

Similar competition between AFM and FM interactions has been reported in Co_3GeN[29] and Co_3SnN,[22] where it is ascribed to SG effects. In Co_3GeN, a canonical SG state arises from atomic disorder caused by Ge vacancies, with a measured Co:Ge ratio of 3.0:0.82. Likewise, in Co_3SnN, SG features are linked either to Sn deficiency or the coexistence of Co–Sn ferromagnetic clusters and Co–N antiferromagnetic interactions, or a combination of both effects. For Co_3ZnN, however, our EPMA measurements indicate a global composition very close to stoichiometric ($Co_{2.97}Zn_{1.01}N_{0.95}O_{0.07}$), suggesting that a large-scale deviation from the expected 3:1:1 stoichiometry is unlikely. Moreover, the presence of the (001) peak in the PXRD data [Fig. 1(a)] implies that the Co and Zn atoms are ordered on their specific sites within the cubic AP structure.

To determine the magnetic ground state, we performed DFT calculations on atomically ordered cubic Co_3ZnN using a supercell approach. We compared collinear FM and AFM configurations using a ten-atom face-centered cubic (fcc) supercell. In this ten-atom cell, the FM state is lower by 30.8 meV/Co than the AFM state considering all ten collinear AFM possibilities; the Co local moment is ∼1 μ_B and the total magnetization is ∼3 μ_B/f.u. We note that other generalized gradient approximation (GGA) studies also report an FM ground state.[30,31] Furthermore, we extended the study to 20-, 40-, and 60-atom supercells and used first-principles Monte Carlo sampling on DFT (based on GGA) energies to search for ground state magnetic configurations (see Methods in the supplementary material). In the 20-atom cell, FM is favored by 26.7 meV per Co, while in the 40-atom cell the energy difference decreases to 12.0 meV per Co; in both larger supercells the AFM solutions converge to zero net magnetization. A larger 60-atom supercell was further modeled, showing a reduced energy difference of 8.9 meV per Co, with the initial AFM configuration relaxing to an FiM state. The systematic reduction in the

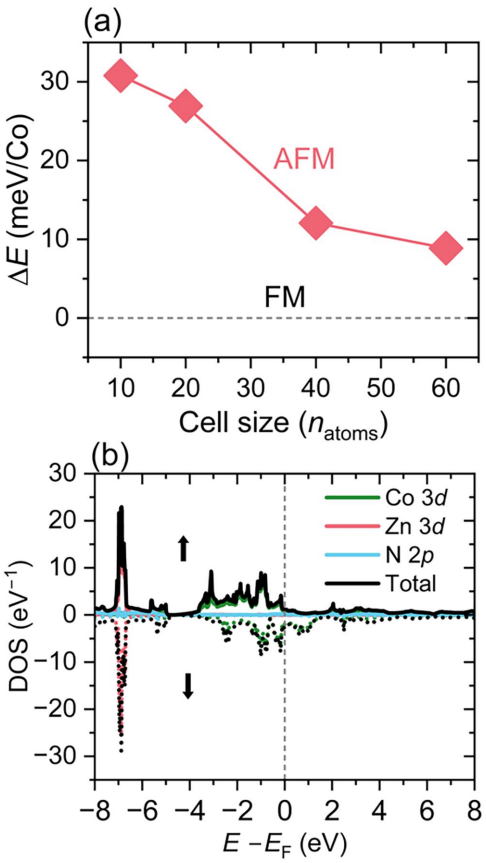

FIG. 3. (a) The collinear energy differences, calculated relative to the FM ground state, show that the competition between FM and AFM states increases with supercell size and (b) the DOS of Co_3ZnN for the FM ground state.

FM–AFM/FiM energy gap with increasing cell size indicates consistent FM ordering but increasing AFM/FiM competition, consistent with frustrated long-range exchange interactions, as shown in Fig. 3(a).

To explore possible non-collinear magnetic states, we performed GGA non-collinear + spin–orbit coupling (SOC) calculations for several candidate structures (AFM-1 Γ_5g,[32] AFM-2 Γ_4g,[33] AFM-3, AFM-4, and an FiM 1:2 up:down configuration), as summarized in Table I. All six non-collinear AFM or FiM configurations are higher in energy

TABLE I. Relative energies of non-collinear magnetic configurations of Co_3ZnN from GGA+SOC calculations.

Magnetic structure	Super-cell size (atoms)	ΔE (meV/Co)
FM	5	0
AFM-1, Γ_{5g}	5	27.5
AFM-2, Γ_{4g}	5	35.8
AFM-3	10	30.7
FiM	10	30.8
AFM-4	40	20.8

than the FM state; the lowest, AFM-4, lies ∼20.8 meV per Co above the FM configuration (compared to 12.0 meV per Co for the collinear 40-atom cell). Thus, within GGA, we can rule out AFM or FiM ground states while recognizing FM–AFM competition, consistent with the collinear results in Fig. 3(a) and the experimental behavior in Fig. 2. The low transition temperature ($T_N = 25$ K), small net moment (0.11 μ_B/f.u.), and weak FM correlations just above the transition in Co_3ZnN support an AFM ground state with competing FM interactions. While strain from growth on STO could induce tetragonal distortion, our films are relaxed; a low-temperature structural transition, however, could modify the energetics, potentially reconciling the observed canted AFM or FiM behavior with the DFT-predicted FM ground state. To further assess possible structural transitions, we performed structure prediction calculations at the GGA level.[34] The FM cubic antiperovskite structure is confirmed as the ground state in both 10- and 20-atom searches.

Overall, the structure search, collinear DFT-based Monte Carlo simulations, and non-collinear calculations consistently indicate an FM ground state. However, we recognize that this is not consistent with the experimental results that indicate a canted AFM or FiM order at 2 K. We note that the energy competition observed in larger supercells, as shown in Fig. 3(a), suggests the possible emergence of more complex AFM or FiM orders at longer length scales. In addition, non-collinear canting, which may not be fully captured in our calculations, could also lead to a magnetic ground state distinct from the ideal FM configuration. Either or both of these effects may be at play in this system, and it is also possible that the cubic structure used for these calculations may not be an accurate representation of the structure of Co_3ZnN near or below its magnetic transition, as the STO substrate, which undergoes a tetragonal phase transition at 105 K, may strain the film.

As shown in Fig. 3(b), the calculated density of states (DOS) confirms the metallic nature of Co_3ZnN. The asymmetric distribution of the spin-resolved DOS near the Fermi energy (E_F), with a larger contribution from the down-spin channel, resembles the behavior reported for Co_3PdN.[24] The Co 3*d* electrons predominantly contribute to the conduction band and exhibit a high DOS near E_F, underscoring their primary role in the electronic and magnetic properties of Co_3ZnN. The Co atoms are primarily responsible for the observed magnetism. In contrast, the Zn *d* states lie far below E_F, suggesting weak electronic hybridization between Co *d*, N *p*, and Zn *d* states and, consequently, weaker FM interactions compared to Co_3PdN.[24]

In conclusion, we synthesized and then successfully studied the structural and magnetic properties of epitaxial Co_3ZnN films. X-ray diffraction confirmed phase-pure (00*l*)-oriented films with cube-on-cube epitaxy and a lattice parameter of 3.752 Å. Magnetic measurements revealed hysteresis at 2 K with a coercive field of ∼0.12 T and a small net moment, indicating a canted AFM or FiM ground state. Temperature-dependent magnetization identified a transition near 25 K and strong AFM interactions with short-range FM correlations. DFT and Monte Carlo simulations predicted an FM ground state, but the narrowing FM–AFM energy difference with increasing cell size suggests competing magnetic interactions. Overall, Co_3ZnN exhibits complex magnetism arising from the interplay of FM and AFM exchange couplings. Idealized DFT favors FM, but real thin-film materials with subtle disorder, distortions, or long-range competing exchange relax into a canted AFM or FiM state.

See the supplementary material for detailed methods and additional XRD and magnetization data.

This work was authored by the National Laboratory of the Rockies for the U.S. Department of Energy (DOE), operated under Contract No. DE-AC36-08GO28308. Funding provided by the U.S. Department of Energy, Office of Science, Basic Energy Sciences, Division of Materials Science, through the Office of Science Funding Opportunity Announcement (FOA) No. DE-FOA-0002676: Chemical and Materials Sciences to Advance Clean-Energy Technologies and Transform Manufacturing. The research used High-Performance Computing (HPC) resources of the National Energy Research Scientific Computing Center (NERSC), a DOE-SC user facility located at Lawrence Berkeley National Laboratory, operated under Contract No. DE-AC02-05CH11231. This research also used HPC resources at NLR, sponsored by the DOE, Office of Critical Minerals and Energy Innovation. The views expressed in the article do not necessarily represent the views of the DOE or the U.S. Government. The authors thank the Analytical Resources Core at Colorado State University for instrument access and training (RRID: No. SCR_021758).

AUTHOR DECLARATIONS

Conflict of Interest

The authors have no conflicts to disclose.

Author Contributions

Sita Dugu: Conceptualization (equal); Formal analysis (equal); Investigation (equal); Methodology (equal); Software (equal); Writing – original draft (equal); Writing – review & editing (equal). **Sharad Mahatara:** Methodology (equal); Software (equal); Writing – original draft (equal). **Corlyn E. Regier:** Methodology (equal). **James R. Neilson:** Supervision (equal); Visualization (equal); Writing – review & editing (equal). **Stephan Lany:** Supervision (equal); Visualization (equal); Writing – review & editing (equal). **Rebecca W. Smaha:** Visualization (equal); Writing – review & editing (equal). **Sage R. Bauers:** Conceptualization (equal); Supervision (equal); Visualization (equal); Writing – review & editing (equal).

DATA AVAILABILITY

The data that support the findings of this study are available from the corresponding authors upon reasonable request and openly available in National Laboratory of the Rockies (NLR), Ref. 35.

REFERENCES

[1]Y. Wang *et al.*, "Antiperovskites with exceptional functionalities," Adv. Mater. **32**(7), 1905007 (2020).
[2]R. Niewa, "Metal-rich ternary perovskite nitrides," Eur. J. Inorg. Chem. **2019**(32), 3647–3660.
[3]B. He *et al.*, "$CuNNi_3$: A new nitride superconductor with antiperovskite structure," Supercond. Sci. Technol. **26**(12), 125015 (2013).
[4]M. Uehara, A. Uehara, K. Kozawa, T. Yamazaki, and Y. Kimishima, "New antiperovskite superconductor $ZnNNi_3$, and related compounds $CdNNi_3$ and $InNNi_3$," Physica C **470**, S688–S690 (2010).
[5]S. Matar, P. Mohn, G. Demazeau, and B. Siberchicot, "The calculated electronic and magnetic structures of Fe_4N and Mn_4N," J. Phys. France **49**(10), 1761–1768 (1988).

[6]C. A. Kuhnen and A. V. dos Santos, "Magnetic and electronic structure of the nitrides $PdFe_3N$ and $MnFe_3N$," J. Magn. Magn. Mater. **130**(1), 353–362 (1994).
[7]P. Mohn, K. Schwarz, S. Matar, and G. Demazeau, "Calculated electronic and magnetic structure of the nitrides $NiFe_3N$ and $PdFe_3N$," Phys. Rev. B **45**(8), 4000–4007 (1992).
[8]C. A. Kuhnen and A. V. dos Santos, "Calculated electronic structure of $SnFe_3N$," Solid State Commun. **85**(3), 273–279 (1993).
[9]S. Suzuki, H. Sakumoto, J. Minegishi, and Y. Omote, "Coercivity and unit particle size of metal pigment," IEEE Trans. Magn. **17**(6), 3017–3019 (1981).
[10]C. A. Kuhnen, R. S. de Figueiredo, V. Drago, and E. Z. da Silva, "Mössbauer studies and electronic structure of γ'-Fe_4N," J. Magn. Magn. Mater. **111**(1), 95–104 (1992).
[11]S. F. Matar, G. Demazeau, and B. Siberchicot, "Magnetic particles derived from iron nitride," IEEE Trans. Magn. **26**(1), 60–62 (1990).
[12]K. Takenaka and H. Takagi, "Giant negative thermal expansion in Ge-doped anti-perovskite manganese nitrides," Appl. Phys. Lett. **87**(26), 261902 (2005).
[13]D. Fruchart and E. F. Bertaut, "Magnetic studies of the metallic perovskite-type compounds of manganese," J. Phys. Soc. Jpn. **44**(3), 781–791 (1978).
[14]J. Yan *et al.*, "Phase transitions and magnetocaloric effect in $Mn_3Cu_{0.89}N_{0.96}$," Acta Mater. **74**, 58–65 (2014).
[15]D. Matsunami, A. Fujita, K. Takenaka, and M. Kano, "Giant barocaloric effect enhanced by the frustration of the antiferromagnetic phase in Mn_3GaN," Nat. Mater. **14**(1), 73–78 (2015).
[16]B. Song *et al.*, "Observation of spin-glass behavior in antiperovskite Mn_3GaN," Appl. Phys. Lett. **92**(19), 192511 (2008).
[17]X. H. Zhang *et al.*, "Observation of spin-glass behavior in antiperovskite compound $Mn_3Cu_{0.7}Ga_{0.3}N$," Appl. Phys. Lett. **103**(2), 022405 (2013).
[18]K. Asano, K. Koyama, and K. Takenaka, "Magnetostriction in Mn_3CuN," Appl. Phys. Lett. **92**(16), 161909 (2008).
[19]B. Wiendlocha, J. Tobola, S. Kaprzyk, and D. Fruchart, "Electronic structure, superconductivity and magnetism study of Cr_3GaN and Cr_3RhN," J. Alloys Compd. **442**(1), 289–291 (2007).
[20]S. Lin *et al.*, "Spin-glass behavior and zero-field-cooled exchange bias in a Cr-based antiperovskite compound $PdNCr_3$," J. Mater. Chem. C **3**(22), 5683–5696 (2015).
[21]H. K. Singh, Z. Zhang, I. Opahle, D. Ohmer, Y. Yao, and H. Zhang, "High-throughput screening of magnetic antiperovskites," Chem. Mater. **30**(20), 6983–6991 (2018).
[22]C. Liu *et al.*, "Spin-glass behavior in Co-based antiperovskite compound $SnNCo_3$," Appl. Phys. Lett. **116**(5), 052401 (2020).
[23]H. Sakakibara, H. Ando, Y. Kuroki, S. Kawai, K. Ueda, and H. Asano, "Magnetic properties and anisotropic magnetoresistance of antiperovskite nitride Mn_3GaN/Co_3FeN exchange-coupled bilayers," J. Appl. Phys. **117**(17), 17D725 (2015).
[24]S. Dugu *et al.*, "Synthesis, stability, and magnetic properties of antiperovskite Co_3PdN," Chem. Mater. **37**(5), 1906–1913 (2025).
[25]Y. Goto, A. Daisley, and J. S. J. Hargreaves, "Towards anti-perovskite nitrides as potential nitrogen storage materials for chemical looping ammonia production: Reduction of Co_3ZnN, Ni_3ZnN, Co_3InN and Ni_3InN under hydrogen," Catal. Today **364**, 196–201 (2021).
[26]H. P. R. Frederikse and G. A. Candela, "Magnetic susceptibility of insulating and semiconducting strontium titanate," Phys. Rev. **147**(2), 583–584 (1966).
[27]W. J. Feng, D. Li, W. J. Ren, Y. B. Li, W. F. Li, J. Li, Y. Q. Zhang, and Z. D. Zhang, "Glassy ferromagnetism in Ni_3Sn-type $Mn_{3.1}Sn_{0.9}$," Phys. Rev. B **73**, 205105 (2025).
[28]L. Zu *et al.*, "A first-order antiferromagnetic-paramagnetic transition induced by structural transition in $GeNCr_3$," Appl. Phys. Lett. **108**(3), 031906 (2016).
[29]L. Zu *et al.*, "Observation of the spin-glass behavior in co-based antiperovskite nitride $GeNCo_3$," Inorg. Chem. **55**(18), 9346–9351 (2016).
[30]H. Hu, X. Yan, X. Wang, C. Yin, J. P. Attfield, and M. Yang, "Magnetic properties and electrocatalytic oxygen evolution performance of a medium-entropy metal nitride," Chem. Mater. **36**(23), 11432–11439 (2024).
[31]S. Liu *et al.*, "Efficient photocatalytic hydrogen evolution over carbon supported antiperovskite cobalt zinc nitride," Chem. Eng. J. **408**, 127307 (2021).
[32]G. Gurung, M. Elekhtiar, Q.-Q. Luo, D.-F. Shao, and E. Y. Tsymbal, "Nearly perfect spin polarization of noncollinear antiferromagnets," Nat. Commun. **15**(1), 10242 (2024).
[33]Z. Miao, X. Guo, G. Yang, N. Wang, and J. Li, "The spin-glass-like behavior in antiperovskite Mn_3AgN," J. Appl. Phys. **136**(5), 055104 (2024).
[34]A. Sharan and S. Lany, "Computational discovery of stable and metastable ternary oxynitrides," J. Chem. Phys. **154**(23), 234706 (2021).
[35]A. Zakutayev *et al.*, "An open experimental database for exploring inorganic materials," Sci. Data **5**(1), 180053 (2018).